Nonsymmetrized Hamiltonian for semiconducting nanostructures in a magnetic field

V. Mlinar,* M. Tadić,† B. Partoens, and F. M. Peeters‡
Departement Fysica, Universiteit Antwerpen (Campus Drie Eiken), Universiteitsplein 1, B-2610 Antwerpen, Belgium
(Received 31 August 2004; revised manuscript received 15 November 2004; published 5 May 2005)

In the framework of the Burt-Foreman theory a nonsymmetrized eight-band effective-mass Hamiltonian is derived for nanostructures in the presence of a magnetic field. The Hamiltonian is tested for the case of a cylindrical quantum dot with parabolic in-plane confinement potential in a perpendicular magnetic field. We compare the results of our nonsymmetrized model to the single-band and conventional multiband calculations, where *ad hoc* symmetrization is used. The model is tested on GaAs/$Al_{0.3}Ga_{0.7}$As, GaAs/AlAs, and InAs/GaAs quantum dots, where strain is not included in the model in order to resolve the influence of the boundary on the electronic structure. In structures with a large difference of Luttinger parameters between the constituent materials, such as InAs/GaAs quantum dots, the conventional multiband models lead to unphysical high magnetic-field solutions that are substantially different from those obtained from the nonsymmetrized Hamiltonian and single-band model for the ground state. A similar behavior is observed for the case of InAs/GaAs quantum wells, where energy levels as a function of k_t are analyzed. This discrepancy is attributed to an overestimation of band mixing in conventional models because of the inappropriate treatment of the boundary.

DOI: 10.1103/PhysRevB.71.205305 PACS number(s): 71.15.−m, 73.21.−b

I. INTRODUCTION

The effective-mass theory is a very well-established method to obtain the band structure in the case of weak perturbing inhomogeneous semiconductor potentials.[1–4] Electron and hole energies near the band extrema in the presence of external magnetic and electric fields and in a crystal containing a shallow impurity were successfully described by this theory.[1,4,5] It is also well suited for valence bands, but because of the degeneracy between the heavy- and light-hole bands, the multiband approach should be applied. The majority of current theoretical work on the calculations of the electronic structure is based on the Luttinger-Kohn Hamiltonian for valence bands and Pidgeon-Brown Hamiltonian to consider mixing between valence and conduction bands. Although the validity of the effective-mass approximation is broken (the weak perturbing potential condition is violated), it has nevertheless been proven to be a useful method to compute the electronic structure of semiconductor nanostructures, owing to its simplicity and reasonable agreement with experiment. For this purpose, the appropriate bulk multiband Hamiltonian is used in each constituent material separately, and the envelope functions on either side of the interface are connected by applying *ad hoc* symmetrization rules.[6] We refer to this approach as the conventional multiband model.

An envelope function theory for nanostructures was developed by Burt.[7] The model is valid for the case of abrupt interfaces and relies only on the slow variation of the envelope functions.[7–9] The fact that the Hamiltonian as a whole is Hermitian, but the matrix elements themselves are not necessarily so, was disregarded in the conventional multiband approach. The operator ordering with respect to the band parameters reflects the boundary conditions at the abrupt interface. This ordering for the nonsymmetrized multiband Hamiltonian was systematically derived by introducing asymmetry parameters, first for quantum wells and superlattices,[10,11] and, subsequently, for an arbitrary three-dimensional confinement in quantum dots.[12]

In the framework of the envelope-function approximation, the problem of the interface in semiconducting nanostructures is very complex and several treatments were recently put forward. General boundary conditions were proposed for the multiband effective-mass theory that required the conservation of the probability flux density normal to the interface and the self-adjointness of the multiband Hamiltonian.[13] Reduced translational and point symmetries of the system due to the interface causes a heavy-hole–light-hole interaction even at the center of the Brillouin zone.[14] It was shown that this anisotropic effect can also be modeled within the Burt-Foreman (BF) theory.[15] Szmulowicz *et al.*[16] developed a modified eight-band envelope-function approximation formalism incorporating this anisotropic effect. The latter effect is not considered in conventional multiband nor in the BF envelope-function approximation. Furthermore, it has been argued that most derivations of effective-mass equations for heterostructures, including Burt's derivation, do not take into account all perturbative corrections up to the same order and that the additional approximation introduced by Foreman,[10] resulting in the asymmetry parameters, was incorrect.[17] Several terms with different operator ordering were omitted, and the asymmetric term in the nonsymmetrized Hamiltonian was found to be incorrect, which lead to the proposal[17] of a different first-principles envelope-function theory. However, the application of the conventional symmetrized Hamiltonian is still widespread and numerous experimental data were described in the framework of this theory, although the treatment of the interface in this model is problematic. Therefore, we implement here the BF theory as a correction to the usual approach. As argued above many subtile effects may not be included, but *no nonphysical solutions* are found within this BF theory, in contrast to the results obtained with the conventional approach.

The electronic structure of unstrained and strained quantum wires and dots has been extensively studied.[18–23] In order to explain experimental results on semiconductor nano-

structures in the presence of a magnetic field,[24] appropriate modeling of the electronic structure is needed. In this paper, we limited ourself to the application of the boundary conditions given in Ref. 25 for the case of a nonzero magnetic field and compare the electronic structure computed by this model to the results of conventional single and multiband models. The presence of such a magnetic field leads to the replacement $\mathbf{k} \rightarrow -i\nabla - e\mathbf{A}/\hbar$, and further to the noncommutivity of different components of $\mathbf{k}$. The fact that different components of $\mathbf{k}$ do not commute was not addressed in the BF approach. In the present paper the nonsymmetrized Hamiltonian for nanostructures and bulk materials in a nonzero magnetic field is derived. A direct relation between the antisymmetric constant κ introduced by Luttinger[4] and the asymmetry parameter[12,25] in the BF model is established. At zero magnetic field, different components of $\mathbf{k}$ commute, and the Hamiltonian of Ref. 12 is recovered.

As an example, we apply the proposed nonsymmetrized Hamiltonian to a cylindrical quantum dot in the presence of a perpendicular magnetic field. The dot confinement potential is, for simplicity, assumed to have parabolic shape in the lateral plane, while along the growth direction (z-axis), a steplike dependence is adopted. Quantum dots formed from $GaAs/Al_{0.3}Ga_{0.7}As$, GaAs/AlAs, and InAs/GaAs, and quantum wells formed from InAs/GaAs are analyzed. In order to fully estimate the influence of the boundary conditions on the electronic structure in InAs/GaAs systems, strain is not taken into account. In such a case, the application of the correct boundary conditions along the z direction is very important. We found that agreement between the nonsymmetrized and conventional models strongly depends on the structural parameters. For systems with a large difference in Luttinger parameters, band mixing in conventional models is found to be overestimated and leads to nonphysical solutions. A good agreement between the single-band model and the nonsymmetrized multiband model for the ground state was observed.

The paper is further organized as follows. The nonsymmetrized Hamiltonian for a finite magnetic field is derived in Sec. II. The details of the electronic structure calculations for cylindrical quantum parabolic in-plane confinement potentials is given in Sec. III. Section IV contains the numerical results. Our results and conclusions are summarized in Sec. V. For completeness we added the strain-dependent part of the Hamiltonian in the Appendix.

II. NONSYMMETRIZED HAMILTONIAN IN AN EXTERNAL MAGNETIC FIELD

In the BF theory, the multiband Hamiltonian for bulk crystals is modified so that:[7,8,10] (i) the operators are ordered with respect to the effective mass parameters, which leads to specific boundary conditions at the atomically abrupt interface; (ii) the light-hole $|3/2,\pm 1/2\rangle$ and the split-off $|1/2,\pm 1/2\rangle$ states are coupled because of the local inversion asymmetry caused by the variation of the material composition.[26]

The Hamiltonian for bulk crystals without spin-orbit coupling written in the basis $|S\rangle$, $|X\rangle$, $|Y\rangle$, $|Z\rangle$ of the periodic parts of the zone-center Bloch functions, is given by[1,25]

$$H_4 = \begin{pmatrix} E_c + A_c k^2 & iPk_x & iPk_y & iPk_z \\ -iPk_x & E_v' - L'k_x^2 - M(k_y^2+k_z^2) & -N'k_xk_y & -N'k_xk_z \\ -iPk_y & -N'k_xk_y & E_v' - L'k_y^2 - M(k_x^2+k_z^2) & -N'k_yk_z \\ -iPk_z & -N'k_xk_z & -N'k_yk_z & E_v' - L'k_z^2 - M(k_x^2+k_y^2) \end{pmatrix}. \tag{1}$$

Here, E_c denotes the energy of the conduction-band minimum, $E_v' = E_v + \Delta/3$, where E_v is the energy of the valence-band maximum and Δ is the spin-orbit split-off energy. P is the Kane matrix element, $L' = (\hbar^2/2m)(\gamma_1 + 4\gamma_2)$, $M = (\hbar^2/2m)(\gamma_1 - 2\gamma_2)$, $N' = (\hbar^2/2m)(6\gamma_3)$, where m is the electron mass. Parameters γ_i are related to the valence-band Luttinger parameters γ_i^L by the relations $\gamma_1 = \gamma_1^L - E_P/3E_g$, $\gamma_2 = \gamma_2^L - E_P/6E_g$, $\gamma_3 = \gamma_3^L - E_P/6E_g$, where E_g is the fundamental band gap, and E_P is related to the Kane matrix element by $E_P = 2mP^2/\hbar^2$. A_c is calculated from the expression $A_c = \hbar^2/2m_c - 2P^2/3E_g - P^2/3(E_g + \Delta)$.

The operator ordering for the zero magnetic field case, proposed in Refs. 10 and 25 is given by:

$$Pk_{x_i} \rightarrow \tfrac{1}{2}(P_1 \hat{k}_{x_i} + \hat{k}_{x_i} P_2), \tag{2}$$

$$Mk_{x_i}^2 \rightarrow \hat{k}_{x_i} M \hat{k}_{x_i}, \tag{3}$$

$$N'k_{x_i}k_{x_j} \rightarrow \hat{k}_{x_i} N_+' \hat{k}_{x_j} + \hat{k}_{x_j} N_- \hat{k}_{x_i}, \tag{4}$$

where $x_i, x_j = x, y, z$; $x_j \neq x_i$. P_1 and P_2 are asymmetry parameters given in the Appendix of Ref. 12. N_+' in Eq. (4) is the contribution to N' from the Γ_1 and Γ_{12} bands, while N_- represents the influence of the Γ_{15} and Γ_{25} bands. If one neglects the Γ_{25} bands, Eq. (4) becomes[25]

$$\hat{k}_{x_i} N_+' \hat{k}_{x_j} + \hat{k}_{x_j} N_- \hat{k}_{x_i} = 3(\hbar^2/2m)(\hat{k}_{x_i}(\gamma_3 + \chi)\hat{k}_{x_j} + \hat{k}_{x_j}(\gamma_3 - \chi)\hat{k}_{x_i}), \tag{5}$$

where χ is called the asymmetry parameter in the notation of Pokatilov *et al.*[12] and is given by $\chi(r) = (2\gamma_2(r) + 3\gamma_3(r) - \gamma_1(r) - 1)/3$.

If the operator ordering, which was proposed in Ref. 25, is implemented in the Hamiltonian for bulk material in the presence of a finite magnetic field[3] ($\mathbf{k}\rightarrow -i\nabla - e\mathbf{A}/\hbar$), it may be shown that the asymmetry parameter, which should only give a contribution at the interface, also contributes away from the interface. As a matter of fact, Eq. (5) can be written as

$$3\frac{\hbar^2}{2m}\Bigg(-i\frac{\partial(\gamma_3+\chi)}{\partial x_i}\hat{k}_{x_j}-i\frac{\partial(\gamma_3-\chi)}{\partial x_j}\hat{k}_{x_i}+\gamma_3\{\hat{k}_{x_i},\hat{k}_{x_j}\} + \chi[\hat{k}_{x_i},\hat{k}_{x_j}]\Bigg). \tag{6}$$

The first two terms represent the correct boundary conditions. They arise from the different contributions of the remote bands of symmetry Γ_1, Γ_{12} (the first term), and Γ_{15} (the second term). In the case of the *ad hoc* symmetrization these two terms also exist but in a different form $3(-i\partial\gamma_3/\partial x_i\hat{k}_{x_j} - i\partial\gamma_3/\partial x_j\hat{k}_{x_i})$, obtained by taking $\chi=0$ in Eq. (5), and they follow from the fact that each matrix element of the Hamiltonian in the *ad hoc* symmetrization has to be Hermitian, which is shown to be incorrect.[7,8,25] The third term represents the anticommutator of the operators $\hat{k}_{x_i}$, $\hat{k}_{x_j}$. Note that both in the *ad hoc* symmetrization and the bulk Hamiltonian, the third term appears. It arises from the symmetry of the crystal.[3,4] The fourth term is the commutator of the operators $\hat{k}_{x_i}$, $\hat{k}_{x_j}$, and it is proportional to the asymmetry parameter χ. It plays a role not only at the boundary but through the whole nanostructure. The correct interpretation of this term is very important. We demonstrate that this term is essentially the same as the one introduced by Luttinger. As analyzed by Luttinger for the case of bulk semiconductors in a magnetic field [see Eq. (12) of Ref. 4], the commutator of different components of $\mathbf{k}$, multiplied by the antisymmetric constant $K/2$ represents the antisymmetric term. As we showed in Eq. (6), in the Burt-Foreman approach this antisymmetric term appears naturally in the derivation and exists in bulk materials as well as in nanostructures. If one compares Eq. (12) of Ref. 4 to Eq. (6) in the case of bulk material [the first two terms in Eq. (6) are then equal to zero], one can obtain a direct relation between the antisymmetric constant K and the asymmetry parameter χ from the BF theory. Note that we treat the conduction band together with the valence bands, so the hole effective masses are written in terms of the scaled Luttinger parameters γ_i (with $i=1,2,3$), as it was shown at the beginning of this section. If one excludes the conduction band from the model, γ_i reduces to γ_i^L, and, as a consequence, χ reduces to $\chi^L=[2\gamma_2^L(r)+3\gamma_3^L(r)-\gamma_1^L(r)-1]/3$. Because of the fact that only the valence bands are treated explicitly in Luttinger's Hamiltonian, K is related to χ^L by $K=-(\hbar^2/m)3\chi^L$. Note that this term vanishes for zero magnetic field when $\hat{k}_{x_i}$, $\hat{k}_{x_j}$ commute. Furthermore, we can relate the asymmetry parameter χ to the dimensionless constant κ, which was introduced by Luttinger: $(\hbar^2/2m)(3\kappa+1)=-K/2$.[4] To be consistent, we denote Luttinger's κ as κ^L. In our case, in which the conduction band is treated together with the valence bands, the scaled κ is related to the Luttinger's κ^L by $\kappa=\kappa^L-E_p/(6E_g)$.[5] The direct relation between κ^L and the asymmetry parameter χ^L from the BF theory is then given by $\kappa^L=\chi^L-1/3$. [Note that it is equivalent to Eq. (23) of Ref. 5 where $\kappa^L=\gamma_3^L+(2/3)\gamma_2^L-(1/3)\gamma_1^L-2/3$.] Inclusion of the conduction band into the model leads to the replacement $\kappa^L\rightarrow\kappa$ and $\chi^L\rightarrow\chi$, resulting in the relation

$$\kappa=\chi-\tfrac{1}{3}, \tag{7}$$

When the spin-orbit interaction is included the basis of the periodic parts of the Bloch functions is given by

$$|1/2,1/2\rangle=|S\uparrow\rangle,$$

$$|1/2,-1/2\rangle=|S\downarrow\rangle,$$

$$|3/2,3/2\rangle=\frac{1}{\sqrt{2}}(|X\uparrow\rangle+i|Y\uparrow\rangle),$$

$$|3/2,1/2\rangle=\frac{i}{\sqrt{6}}(|X\downarrow\rangle+i|Y\downarrow\rangle-2|Z\uparrow\rangle),$$

$$|3/2,-1/2\rangle=\frac{1}{\sqrt{6}}(|X\uparrow\rangle-i|Y\uparrow\rangle-2|Z\downarrow\rangle),$$

$$|3/2,-3/2\rangle=\frac{i}{\sqrt{2}}(|X\downarrow\rangle+i|Y\downarrow\rangle),$$

$$|1/2,1/2\rangle=\frac{1}{\sqrt{3}}(|X\downarrow\rangle+i|Y\downarrow\rangle+|Z\uparrow\rangle),$$

$$|1/2,-1/2\rangle=\frac{-i}{\sqrt{3}}(|X\uparrow\rangle-i|Y\uparrow\rangle-|Z\downarrow\rangle). \tag{8}$$

In the single-group representation the $\Gamma_8\times\Gamma_8$ parameters γ_1, γ_2, γ_3, and κ also involve the split-off band Γ_7, and this representation is the one that we will use. However, in the full double-group picture the $\Gamma_7\times\Gamma_7$ and $\Gamma_7\times\Gamma_8$ parameters are independent of the $\Gamma_8\times\Gamma_8$ ones.[2] Following the procedure by Weiler *et al.*[2] the complete 8×8 nonsymmetrized Hamiltonian is given by

$$\hat{H} = \begin{pmatrix}
D_{cb+} & C_{N-} + 2\left(N_1 + \frac{1}{2}\right)H_- & iV_+ & \sqrt{\frac{2}{3}}V_0 & (i/\sqrt{3})V_- & 0 & (i/\sqrt{3})V_0 & \sqrt{\frac{2}{3}}V_- \\
C_{N+} + 2\left(N_1 + \frac{1}{2}\right)H_+ & D_{cb-} & 0 & -\frac{1}{\sqrt{3}}V_+ & i\sqrt{\frac{2}{3}}V_0 & -V_- & i\sqrt{\frac{2}{3}}V_+ & -\frac{1}{\sqrt{3}}V_0 \\
-iV_+^\dagger & 0 & D_{hh+} & -S_- - i\frac{7}{4}\sqrt{3}C_{q-} - i\sqrt{3}\left(\kappa + \frac{7}{4}q\right)H_- & -R & \frac{3}{2}i(C_{q+} + qH_+) & -(i/\sqrt{2})S_- + \sqrt{\frac{3}{2}}(1+\kappa)H_- & i\sqrt{2}R \\
\sqrt{\frac{2}{3}}V_0^\dagger & -\frac{1}{\sqrt{3}}V_1^\dagger & -S_-^\dagger + i\frac{7}{4}\sqrt{3}C_{q+} + i\sqrt{3}\left(\kappa + \frac{7}{4}q\right)H_+ & D_{lh+} & -C - 2i\frac{5}{2}C_{q-} - i2\left(\kappa + \frac{5}{2}q\right)H_- & -R & i\sqrt{2}(Q_+ + H_z) & -i\sqrt{\frac{3}{2}}\Sigma_- - \sqrt{\frac{1}{2}}(1+\kappa)H_- \\
-(i/\sqrt{3})V_-^\dagger & -i\sqrt{\frac{2}{3}}V_0^\dagger & -R^\dagger & -C^\dagger + 2i\frac{5}{2}C_{q+} + i2\left(\kappa + \frac{5}{2}q\right)H_+ & D_{lh-} & S_+^\dagger - i\sqrt{3}\frac{7}{4}C_{q-} - i\sqrt{3}\left(\kappa + \frac{7}{4}q\right)H_- & i\sqrt{\frac{3}{2}}\Sigma_+ + \sqrt{\frac{1}{2}}(1+\kappa)H_+ & i\sqrt{2}(Q_- - H_z) \\
0 & -V_-^\dagger & -\frac{3}{2}i(C_{q-} + qH_-) & -R^\dagger & S_+ + i\sqrt{3}\frac{7}{4}C_{q+} + i\sqrt{3}\left(\kappa + \frac{7}{4}q\right)H_+ & D_{hh-} & i\sqrt{2}R^\dagger & (i/\sqrt{2})S_+ - \sqrt{\frac{3}{2}}(1+\kappa)H_+ \\
-(i/\sqrt{3})V_0^\dagger & -i\sqrt{\frac{2}{3}}V_+^\dagger & (i/\sqrt{2})S_-^\dagger + \sqrt{\frac{3}{2}}(1+\kappa)H_+ & -i\sqrt{2}(Q_+ + H_z)^\dagger & -i\sqrt{\frac{3}{2}}\Sigma_+^\dagger + \sqrt{\frac{1}{2}}(1+\kappa)H_- & -i\sqrt{2}R & D_{so+} & C + i2\left(\frac{1}{2} + \kappa\right)H_- \\
\sqrt{\frac{2}{3}}V_-^\dagger & \frac{1}{\sqrt{3}}V_0^\dagger & -i\sqrt{2}R^\dagger & i\sqrt{\frac{3}{2}}\Sigma_-^\dagger - \sqrt{\frac{1}{2}}(1+\kappa)H_+ & -i\sqrt{2}(Q_- - H_z)^\dagger & -(i/\sqrt{2})S_+^\dagger - \sqrt{\frac{3}{2}}(1+\kappa)H_- & C^\dagger - i2\left(\frac{1}{2} + \kappa\right)H_+ & D_{so-}
\end{pmatrix}. \tag{9}$$

where

$$D_{cb\pm} = E_c + T \pm \frac{\hbar^2}{2m}(2N_1+1)i[\hat{k}_x,\hat{k}_y] \pm 2iC_{N_{1_z}}, \quad (10)$$

$$D_{hh\pm} = E_v - (P_\pm + Q_\pm) \mp \frac{\hbar^2}{2m}3(\kappa + (9/4)q)i[\hat{k}_x,\hat{k}_y] \mp (27/4)iC_{q_z},$$

$$D_{lh\pm} = E_v - (P_\pm - Q_\pm) \mp \frac{\hbar^2}{2m}[\kappa + (1/4)q]i[\hat{k}_x,\hat{k}_y] \mp (1/4)iC_{q_z},$$

$$D_{so\pm} = E_v - \Delta - P_\pm \mp \frac{\hbar^2}{2m}(2\kappa+1)i[\hat{k}_x,\hat{k}_y],$$

$$\hat{k}_+ = \frac{\hat{k}_x + i\hat{k}_y}{\sqrt{2}}, \quad \hat{k}_- = \frac{\hat{k}_x - i\hat{k}_y}{\sqrt{2}}, \quad (11a)$$

$$H_z = \frac{\hbar^2}{2m}(1+\kappa)[\hat{k}_x,\hat{k}_y], \quad (11b)$$

$$H_\pm = \pm\frac{\hbar^2}{2m}\sqrt{2}[k_\pm,k_z], \quad (11c)$$

$$V_\pm = \frac{1}{2}(P_1\hat{k}_\pm + \hat{k}_\pm P_2), \quad (11d)$$

$$V_0 = \frac{1}{2}(P_1\hat{k}_z + \hat{k}_z P_2), \quad (11e)$$

$$T = \hat{k}_+ A_c \hat{k}_- + \hat{k}_- A_c \hat{k}_+ + \hat{k}_z A_c \hat{k}_z, \quad (11f)$$

$$P_\pm = \frac{\hbar^2}{2m}(\gamma_1\{\hat{k}_\pm,\hat{k}_\mp\} + [\hat{k}_\pm(\gamma_1 - 2\chi)]\hat{k}_\mp + [\hat{k}_\mp(\gamma_1+2\chi)]\hat{k}_\pm + \hat{k}_z\gamma_1\hat{k}_z), \quad (11g)$$

$$Q_\pm = \frac{\hbar^2}{2m}(\gamma_2\{\hat{k}_\pm,\hat{k}_\mp\} + [\hat{k}_\pm(\gamma_2 - \chi)]\hat{k}_\mp + [\hat{k}_\mp(\gamma_2+\chi)]\hat{k}_\pm - 2\hat{k}_z\gamma_2\hat{k}_z), \quad (11h)$$

$$R = \sqrt{3}\frac{\hbar^2}{2m}[\hat{k}_+(\gamma_2 - \gamma_3)\hat{k}_+ + \hat{k}_-(\gamma_2+\gamma_3)\hat{k}_-], \quad (11i)$$

$$S_\pm = \pm i\sqrt{6}\frac{\hbar^2}{2m}(\gamma_3\{\hat{k}_\pm,\hat{k}_z\} + [\hat{k}_\pm(\gamma_3+\chi)]\hat{k}_z + [\hat{k}_z(\gamma_3-\chi)]\hat{k}_\pm), \quad (11j)$$

$$\Sigma_\pm = \pm i\sqrt{6}\frac{\hbar^2}{2m}\left\{\gamma_3\{\hat{k}_\pm,\hat{k}_z\} + \left[\hat{k}_\pm\left(\gamma_3 - \frac{\chi}{3}\right)\right]\hat{k}_z + \left[\hat{k}_z\left(\gamma_3+\frac{\chi}{3}\right)\right]\hat{k}_\pm\right\}, \quad (11k)$$

$$C = -i2\sqrt{2}\frac{\hbar^2}{2m}[(\hat{k}_-\chi)\hat{k}_z - (\hat{k}_z\chi)\hat{k}_-]. \quad (11l)$$

$$C_{q\pm} = \pm\sqrt{2}\frac{\hbar^2}{2m}[(\hat{k}_\pm q)\hat{k}_z - (\hat{k}_z q)\hat{k}_\pm]. \quad (12a)$$

$$C_{q_z} = \frac{\hbar^2}{2m}[(\hat{k}_x q)\hat{k}_y - (\hat{k}_y q)\hat{k}_x]. \quad (12b)$$

$$C_{N_{1^\pm}} = \pm 2\sqrt{2}\frac{\hbar^2}{2m}[(\hat{k}_\pm N_1)\hat{k}_z - (\hat{k}_z N_1)\hat{k}_\pm]. \quad (12c)$$

$$C_{N_{1_z}} = \frac{\hbar^2}{2m}[(\hat{k}_x N_1)\hat{k}_y - (\hat{k}_y N_1)\hat{k}_x]. \quad (12d)$$

N_1 contributes to the electron g factor,[2] and q is the parameter introduced by Luttinger.[4] Because of a reduced symmetry at the interface, also an additional coupling is caused by these parameters q and N_1 at the interface. It is included in the Hamiltonian Eq. (9) through $C_{q\pm}$, C_{q_z}, $C_{N_{1^\pm}}$, and $C_{N_{1_z}}$ given by Eqs. (12), but in our numerical calculations in Sec. IV, we assume that these two parameters are zero.

In Eq. (9) † denotes Hermitian conjugation. We avoided using complex conjugation of operators and transposition of operators, as presented in Ref. 12, because in the magnetic-field case it would lead to incorrect results. Without magnetic field $\hat{k}^*_{x_i} = -\hat{k}_{x_i}$ and $\hat{k}^*_\pm = -\hat{k}_\mp$, but in the case of magnetic field $\hat{k}^*_{x_i} \neq -\hat{k}_{x_i}$ and $\hat{k}^*_\pm \neq -\hat{k}_\mp$. We adopt the convention introduced by Foreman.[10]

In Eqs. (11g) and (11h) $\{\hat{k}_\pm,\hat{k}_\mp\} = \hat{k}_\pm\hat{k}_\mp + \hat{k}_\mp\hat{k}_\pm$, and in Eqs. (11j) and (11k) $\{\hat{k}_\pm,\hat{k}_z\} = \hat{k}_\pm\hat{k}_z + \hat{k}_z\hat{k}_\pm$.

In the case of a nanostructure in a perpendicular magnetic field, the Zeeman terms on the diagonal and those that couple light-hole and split-off bands remain, and all others become zero. This case will be considered in Sec. III, where a cylindrical quantum dot in a perpendicular magnetic field is analyzed. For completeness, the Hamiltonian for strained semiconducting nanostructures is addressed in the Appendix, where the explicit terms of the strain-dependent part of the Hamiltonian are given.

If the asymmetry parameter χ is taken equal to zero, this Hamiltonian has the same form as the conventional 8×8 multiband Hamiltonian for the magnetic-field case.

III. ELECTRONIC STRUCTURE CALCULATIONS

In order to test the nonsymmetrized Hamiltonian, we calculate the electronic structure of a cylindrical quantum dot with parabolic in-plane confinement potential and compare the results to those of the conventional multiband models. A hard-wall potential of rectangular shape is assumed along the z direction, and the case of a perpendicular magnetic field is considered. The axial approximation is adopted. It corresponds to ignoring the square terms that are not axially symmetric about the z-axis [Eq. (11i)]. Since the confinement potential has cylindrical symmetry, the z component of the

total angular momentum $\mathbf{F}$ can be introduced as a good quantum number, $\mathbf{F}_z = f_z\hbar$.[27,28] The z projection of the total angular momentum $\mathbf{F}$ can be written as $\mathbf{F}_z = \mathbf{J}_z + \mathbf{L}_z$, where $\mathbf{J}_z$ is the z component of the angular momentum of the band-edge Bloch function and $\mathbf{L}_z$ is the z component of the envelope angular momentum. In the presence of a magnetic field, the operators $k_\pm$, take the form

$$k_\pm = -ie^{i\varphi}\left(\frac{\partial}{\partial\rho} \pm \frac{i}{\rho}\frac{\partial}{\partial\varphi} \mp \frac{\rho}{2l_c^2}\right), \tag{13}$$

in cylindrical coordinates. Here l_c is the magnetic length given by $l_c = (\hbar/eB)^{1/2}$.

The states are described by the Hamiltonian

$$H = H_{\text{kin}} + V(\rho, z), \tag{14}$$

where H_{kin} presents the kinetic part given in Eq. (9) and $V(\rho,z)$ is a diagonal matrix containing potentials for the valence and conduction band. For $GaAs/Al_{0.3}Ga_{0.7}As$ the eight-band effective mass Hamiltonian is employed, whereas for GaAs/AlAs, InAs/GaAs we use the six-band effective-mass Hamiltonian. AlAs is indirect-gap semiconductor, so coupling between the valence and conduction band cannot be modeled by the 8×8 Hamiltonian. In the case of an InAs/GaAs quantum dot, the full picture can be obtained by employing the 8×8 Hamiltonian.[21] But here, we are interested in the influence of the boundary conditions on the electronic structure calculations of the valence band. In order to analyze the influence of the boundary conditions we have already excluded the strain from our calculations. For the valence band the boundary conditions extracted from the conventional approach are significantly different from those extracted from the nonsymmetrized one. By resolving the problem one gets a more precise treatment of the abrupt interface in the framework of the BF multiband effective-mass theory for the valence band and one could further incorporate these boundary conditions in the full 8×8 nonsymmetrized Hamiltonian. It should be pointed out that generalized envelope-function theory should include additional material parameters, whose values can be obtained from the first-principles calculations or experiments on heterostructures.

For the parabolic quantum dot, $V(\rho,z) = V_\parallel(\rho) + V_\perp(z)$, where $V_\parallel(\rho)$ and $V_\perp(z)$ are given by

$$V_\parallel(\rho) = \tfrac{1}{2}\omega_0^2 m_i \rho^2, \tag{15}$$

$$V_\perp(z) = \begin{cases} \Delta E_i & \text{for } |z| > h/2, \\ 0 & \text{for } |z| < h/2. \end{cases} \tag{16}$$

where $i = c, h$, m_c is the electron mass, $m_h = m_0/(\gamma_1+\gamma_2)$ is the heavy-hole mass, and ω_0 is the characteristic frequency of the lateral confinement potential.

If the quantum dot is symmetric in the z direction, the parity of the wave function is a good quantum number. The spinor of the even valence-band state has the form[23]

$$F_+ = [F_{cb}^+, F_{cb}^-, F_{hh}^+, F_{lh}^-, F_{lh}^+, F_{hh}^-, F_{so}^-, F_{so}^+], \tag{17}$$

The states, for a given quantum number f_z, are denoted by $nX_{f_z}^{\text{par}}$ (Ref. 28), where n is the label of the state for given f_z, X denotes the states with lowest $|l|$ among bands in the basis, and "par" represents the total parity of the state (+ for even parity, − for odd parity). It is obvious that crossings between states of the same total parity and the same f_z are forbidden because of the fact that states are classified with respect to f_z, parity, and n. The ordering of the even and odd states depends on the dimensions of the quantum dot.

The envelope functions in both the valence and conduction bands are expanded into

$$\chi_{n,l,s}^{\pm} = C(n,l,s)\Phi_{nl}(\rho,\varphi)f_s^{\pm}(z). \tag{18}$$

The in-plane part is given by

$$\Phi_{nl}(\rho,\varphi) = \frac{1}{\sqrt{2\pi}}\exp(il\varphi)\exp(-\rho^2/2a^2)\left(\frac{\rho}{a}\right)^{|l|} L_n^{|l|}(\rho^2/a^2), \tag{19}$$

while the z-dependent part is given by

$$f_s^+(z) = \frac{1}{\sqrt{L_z}}\cos\frac{m\pi z}{2L_z}, \quad m = 1,3,5,\cdots, \tag{20}$$

$$f_s^-(z) = \frac{1}{\sqrt{L_z}}\sin\frac{m\pi z}{2L_z}, \quad m = 2,4,6,\cdots \tag{21}$$

In Eqs. (18)–(21), $C(n,l,s)$ is a normalization constant, $L_n^l(x)$ is the generalized Laguerre polynomial, L_z denotes the half-height of the expansion cylinder, and l is computed for the given f and j. The length a is related to the magnetic length l_c and the harmonic length l_0 [$l_0 = (\hbar/\omega_0 m_h)^{1/2}$] through $a = (2l_0^2 l_c^2)/(l_0^4 + 4l_c^4)^{1/2}$. We assumed a step variation of the material parameters, for example, for $\gamma_i = \gamma_{im} + (\gamma_{id} - \gamma_{im})[\theta(z+w) - \theta(z-w)]$, where index m denotes the value of the Luttinger parameter in the matrix and index d the value of this parameter in the dot, w is the half-height of the dot and θ is the Heaviside step function.

TABLE I. Material parameters used in the electronic structure calculations (from Ref. 29).

	GaAs	AlAs	InAs
m_c^*/m_0	0.067	0.15	0.026
γ_1^L	6.98	3.76	20.00
γ_2^L	2.06	0.82	8.5
γ_3^L	2.93	1.42	9.2
κ^L	1.28	0.12	7.68
Δ_0 (eV)	0.341	0.28	0.39
E_g (eV)	1.519		0.417
E_P (eV)	28.8	21.1	21.5

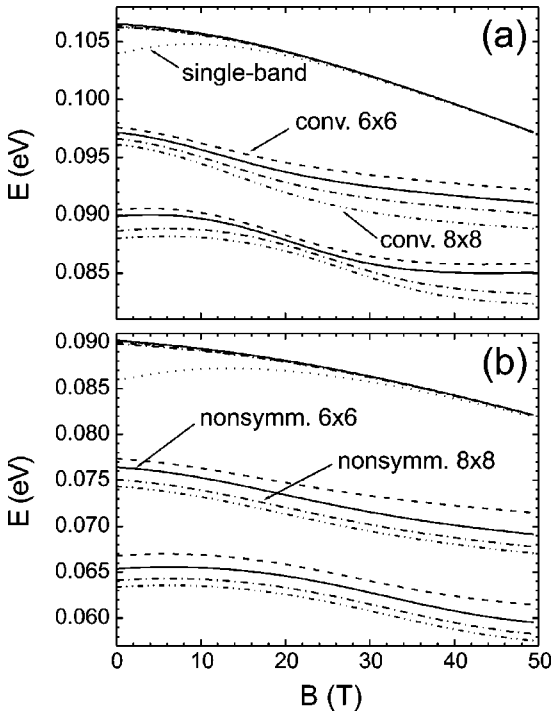

FIG. 1. The three lowest-hole energy levels of $S^{+}_{-3/2}$ symmetry in a $GaAs/Al_{0.3}Ga_{0.7}As$ quantum disk as a function of the magnetic field: (a) $\hbar\omega_0=10$ meV, $h=6$ nm, (b) $\hbar\omega_0=15$ meV, and $h=4$ nm.

IV. NUMERICAL RESULTS AND DISCUSSION

The energy levels of the holes are computed as they vary with the magnetic field for a range of confinement strengths and thicknesses of the cylindrical quantum dot. The band-structure parameters are given in Table I. The half-height of the expansion cylinder is assumed to be approximately four times bigger than the half-height of the dot. Eight in-plane and 40 z-dependent basis functions were employed in the calculation. If the basis size is increased, the energy levels shift by less than 0.8 meV. We tested the nonsymmetrized 8×8 multiband Hamiltonian by comparing the energy levels to those extracted from the respective conventional one. Also, 6×6 multiband nonsymmetrized and conventional models are compared. The difference between the nonsymmetrized and the conventional Hamiltonian arises from the different treatment of the interface in these approaches. As previously discussed, the asymmetry parameter arises at the interface and contributes to the effective mass parameters in the nonsymmetrized Hamiltonian, whereas in the conventional Hamiltonian this parameter equals zero. Consequently, we expect that agreement between these models strongly depends on the structural parameters, and therefore we compare these two models as a function of the magnetic field for different materials in the dot and the barrier.

The magnetic-field dependence of the three lowest-hole energy levels of $S^{+}_{-3/2}$ symmetry in a $GaAs/Al_{0.3}Ga_{0.7}As$ quantum dot is shown in Fig. 1. The 6×6 and 8×8 nonsymmetrized and conventional Hamiltonians are compared. With varying in-plane confinement potential as well as height of the dot, the two models give similar results, but note that the discrepancy between the two models is larger for the more strongly confined quantum dot [Fig. 1(b)]. By explicitly including the lowest conduction band (8×8 model), results do not change qualitatively with respect to those from the 6×6 model (Fig. 1). For the analyzed quantum dot the lowest-hole energy levels for 16 different symmetries are shown in Fig. 2, obtained by the 6×6 nonsymmetrized multiband Hamiltonian. The expected behavior of energy levels as a function of magnetic field is observed, and it was already analyzed in Ref. 28.

For GaAs/AlAs we used only the 6×6 nonsymmetrized and conventional Hamiltonians. Energy levels of holes as a function of magnetic field are shown in Fig. 3. In this case the difference in Luttinger parameters in the dot and barrier is larger than in $GaAs/Al_{0.3}Ga_{0.7}As$ (see Table I), and we note that the difference between the two approaches becomes more pronounced. However, the energy level behavior as a function of the magnetic field is qualitatively the same, only an energy shift is observed.

There is a good qualitative agreement between these two models and the single band model (dotted lines in Figs. 1 and 3) for the ground state, in both $GaAs/Al_{0.3}Ga_{0.7}As$ and GaAs/AlAs as well. However, in the case of a large in-plane confinement potential, when band mixing becomes more important, the discrepancy in the results obtained by the single and multiband models is more pronounced [see Figs. 1(b) and 3(b)]. Another discrepancy is also observed for low values of the magnetic field. The Zeeman energy term in the single-band model tends to decrease the energy, but with increasing the value of the magnetic field the kinetic energy

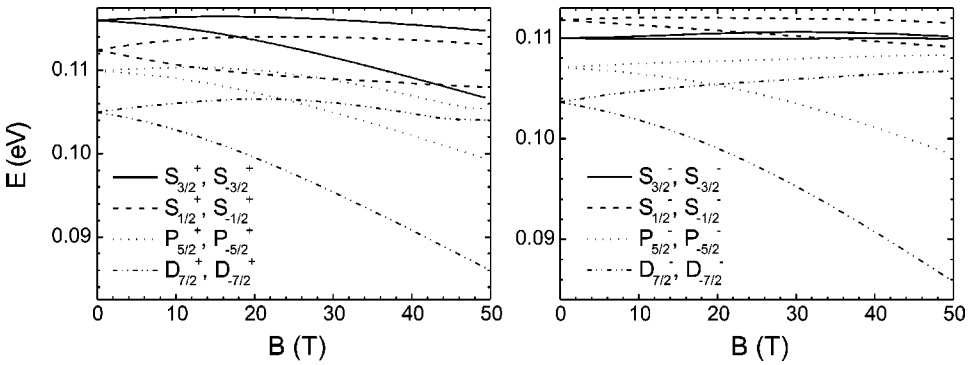

FIG. 2. The lowest hole energy levels for sixteen different symmetries as a function of the magnetic field in $GaAs/Al_{0.3}Ga_{0.7}As$ quantum dot: $\hbar\omega_0=10$ meV and $h=10$ nm. The results are given for the 6×6 nonsymmetrized multiband Hamiltonian.

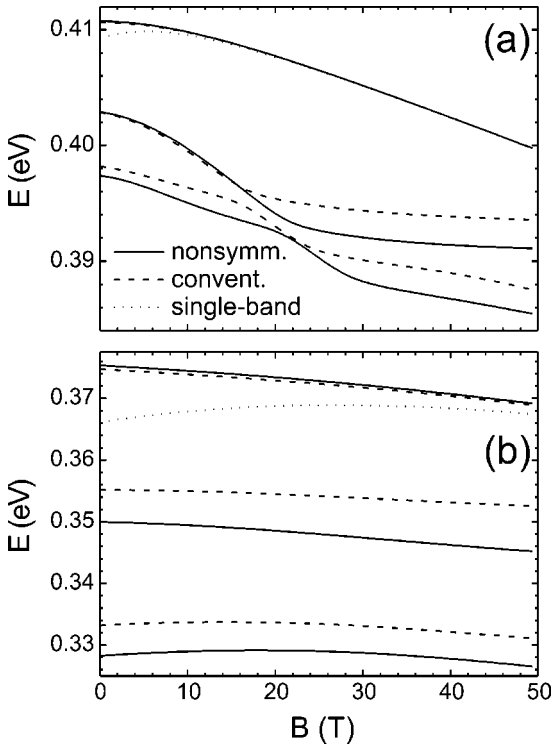

FIG. 3. The three lowest-hole energy levels of $S^{+}_{-3/2}$ symmetry as a function of the magnetic field in a GaAs/AlAs quantum dot: (a) $\hbar\omega_0=6$ meV, $h=6$ nm and (b) $\hbar\omega_0=30$ meV, $h=4$ nm.

part becomes dominant, which further leads to the expected behavior of the energy level as a function of the magnetic field. In the multiband model, however, band mixing plays an important role, and it partially suppresses the effect of the Zeeman energy term. For high values of the magnetic field, a full agreement between the results of the single and multiband models for the ground state is obtained.

Next we consider the case of an InAs/GaAs quantum dot in a magnetic field. The results are shown in Figs. 4(a) and 4(b), which exhibit the ground and first excited hole energy level in a quantum disk with $\hbar\omega_0=6$ meV and $\hbar\omega_0=10$ meV, respectively. In order to fully resolve the influence of the boundary on the electronic structure, strain was not included in the model although the lattice mismatch is 6.8%. The effect of strain will be addressed at the end of this section. Results obtained by the nonsymmetrized Hamiltonian and the single-band model show good agreement, but those obtained by the conventional models differ appreciably. For high values of the magnetic field, the values of the energy levels obtained in the framework of conventional $\mathbf{k}\cdot\mathbf{p}$ theory, become unphysical. Indeed, note that for the $h=10$ nm high dot (Fig. 4), and for values of the magnetic field $B\geqslant 27$ T, the energy levels lie above the top of the valence band. With increasing height of the dot, the effect of the interface boundary becomes less important, and, consequently, the difference between the energies computed by the different models becomes smaller. Only when the quantum dot thickness is

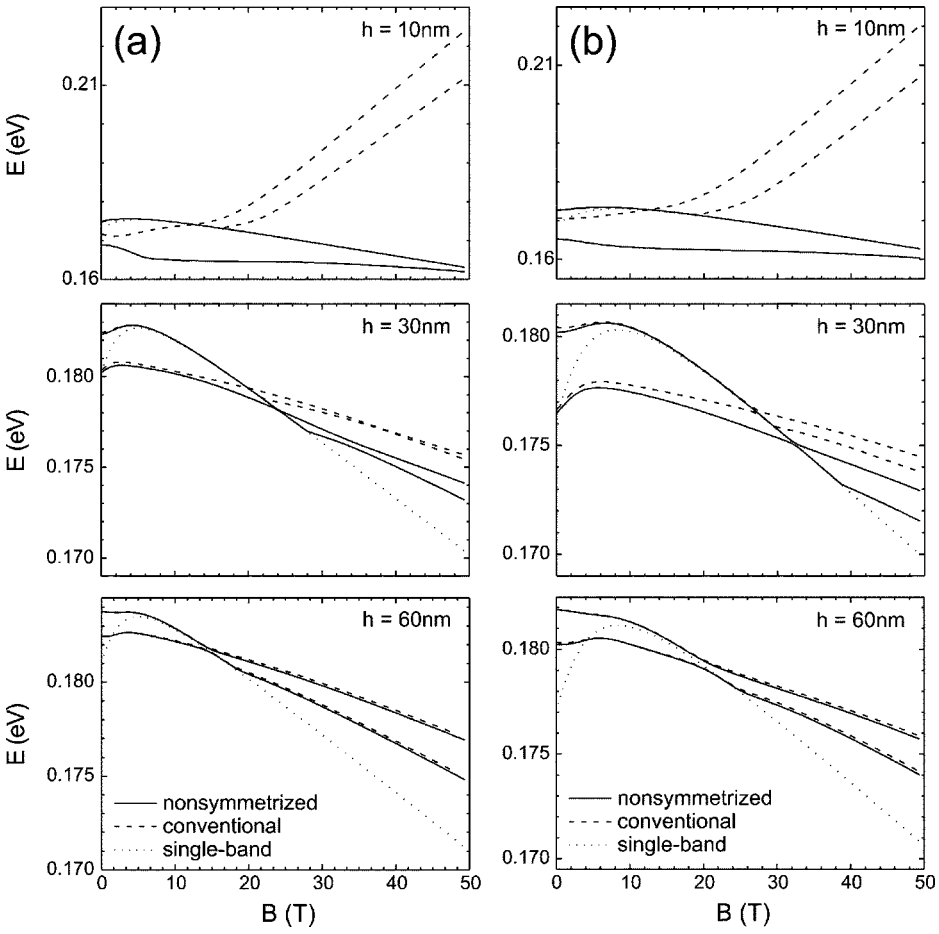

FIG. 4. The two lowest-hole energy levels of $S^{+}_{-3/2}$ symmetry as a function of a magnetic field in InAs/GaAs. Results obtained by the 6×6 nonsymmetrized Hamiltonian (solid line), and by the 6×6 conventional Hamiltonian (dashed line). The height of the dot varies from 10 to 60 nm: (a) $\hbar\omega_0=6$ meV and (b) $\hbar\omega_0=10$ meV.

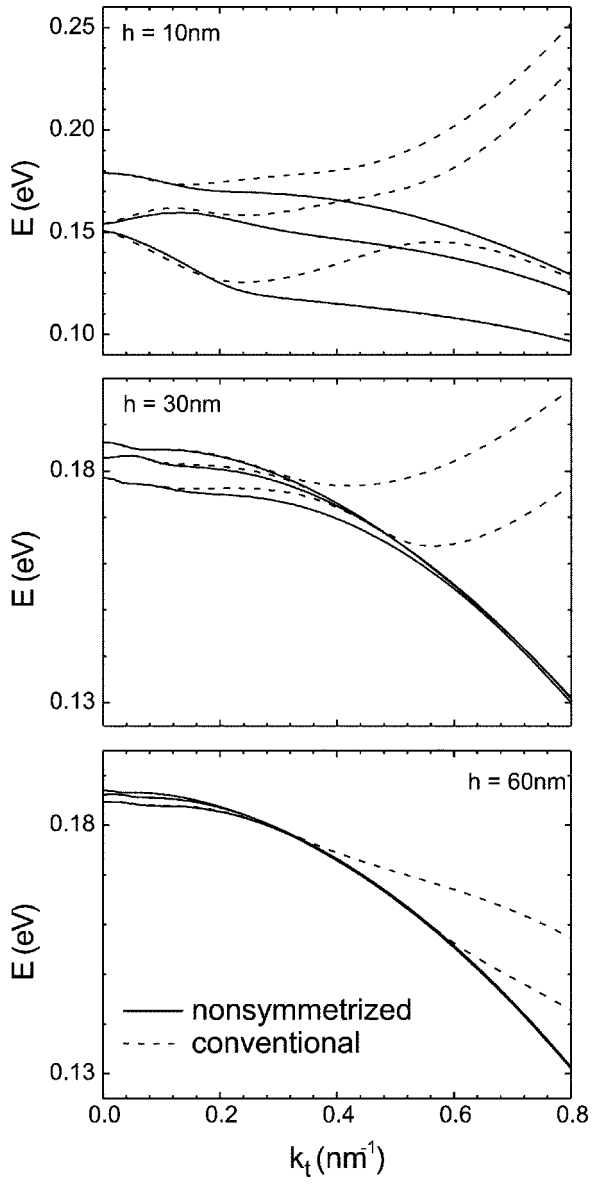

FIG. 5. The three lowest-hole energy levels of InAs/GaAs quantum well as a function of k_t. Results are given for the nonsymmetrized Hamiltonian (solid line) and the conventional 6×6 Hamiltonian (dashed line). The width of the well varies from 10 to 60 nm.

larger than ~60 nm, the results obtained by the two models become identical in the considered magnetic field range. We found that such a behavior is due to the S element in the Hamiltonian

$$S_{\pm} = \pm i\sqrt{6}\frac{\hbar^2}{2m}\left[2\gamma_3\hat{k}_z - i\frac{d(\gamma_3-\chi)}{dz}\right]\hat{k}_{\pm}. \tag{22}$$

The influence of the boundary on the "conventional" S element is determined by the factor $d(\gamma_3-\chi)/dz$ in Eq. (22) and is $(\gamma_{3_d}-\gamma_{3_m})/[(\gamma_{3_d}-\chi_d)-(\gamma_{3_m}-\chi_m)]\approx 135$ times larger than in the nonsymmetrized S element for the InAs/GaAs dot under study. As a consequence, band mixing is overestimated in the conventional Hamiltonian, which is large for materials with a large difference in Luttinger parameters. This overestimation leads to nonphysical solutions for high magnetic-field values, as $d(\gamma_3-\chi)/dz$ is multiplied by $k_{\pm}$ in Eq. (22), which depends on the magnetic field. Note that any other dependence of $\hat{k}_{\pm}$ (e.g., on the parabolic confinement strength) will cause such an amplification as well. The same behavior can be expected in the more simple case of a quantum well in the absence of a magnetic field, where $\hat{k}_{\pm}\rightarrow k_{\pm}$ is now a number. In this case we calculate the hole energy levels as a function of k_t ($k_t=\sqrt{k_x+k_y}$). This is shown in Fig. 5 for quantum well growth in the [001] direction. In this case, k_t artificially amplifies the effect of the boundary and also leads to nonphysical solutions, i.e., the energy levels for high values of k_t lie above the top of the valence band. It should be pointed out that this comparison was made just to illustrate the influence of the boundary on the electronic structure calculations for nanostructures and to stress that the observed nonphysical solutions as a function of a magnetic field for a quantum dot in a magnetic field are a consequence of the ill-defined boundary conditions at the abrupt interface.

In order to illustrate the difference between the conventional and nonsymmetrized approaches, the probability densities in the ground state at $B=40$ T for the InAs/GaAs quantum dot and at $k_t=0.5$ nm^{-1} for the InAs/GaAs quantum well determined by the nonsymmetrized and conventional

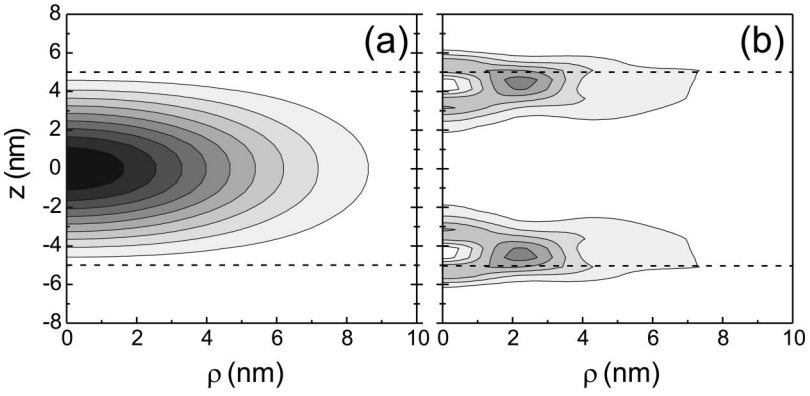

FIG. 6. The probability density of the $1S^{+}_{-3/2}$ state, $\hbar\omega_0=10$ meV, calculated for InAs/GaAs using the (a) nonsymmetrized Hamiltonian and (b) conventional Hamiltonian, for a magnetic field of $B=40$ T. The darker region denotes higher probability density.

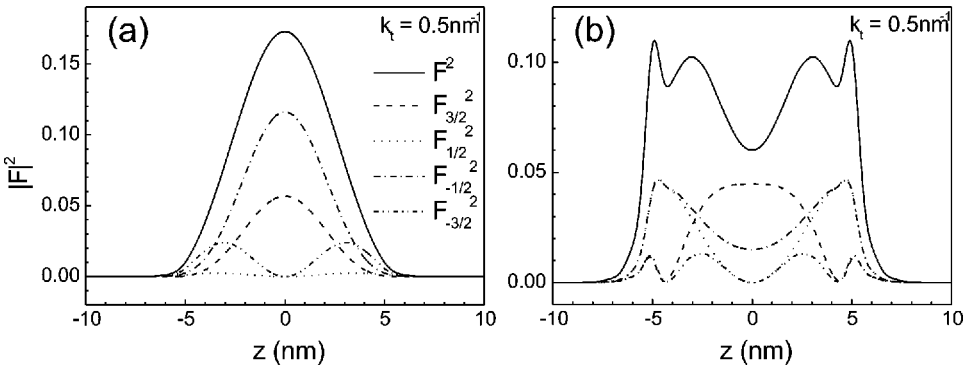

FIG. 7. The probability density for the InAs/GaAs quantum well case at $k_t = 0.5\ \mathrm{nm}^{-1}$ using the (a) nonsymmetrized Hamiltonian and (b) conventional Hamiltonian. Contributions of the different heavy- and light-hole components are also shown.

Hamiltonians are shown in Figs. 6 and 7, respectively. Note that the state shown in Fig. 6(a) is heavy holelike, which explains the good agreement between the single-band and nonsymmetrized models displayed in Fig. 4. In the conventional approach, however, there is a strong mixing between the heavy and light hole, and the holes are localized near the boundaries in the *z* direction. One can note a similar behavior in the quantum well case, where holes, according to the conventional approach, are also localized near the boundary (Fig. 7).

Let us also briefly discuss the results for the single-band model for the InAs/GaAs quantum dot. These conclusions obtained previously from the comparison of the single- and multiband models for $GaAs/Al_{0.3}Ga_{0.7}As$ and GaAs/AlAs are valid for the InAs/GaAs quantum dot as well. However, in the latter case the discrepancy between the single-band and nonsymmetrized multiband models, as found with increasing height of the dot, appears at higher magnetic field. This is a consequence of the lower spatial confinement in the *z* direction, which leads to a relatively stronger influence of the in-plane part and band mixing caused by the magnetic field. Note that by increasing the value of the confinement potential from $\hbar\omega_0 = 6$ meV [Fig. 4(a)] to $\hbar\omega_0 = 10$ meV [Fig. 4(b)], the influence of the magnetic field is reduced and therefore the discrepancy between single- and multiband models appears at higher values of the magnetic field.

For completeness, the lowest-hole energy levels for 16 different symmetries are shown in Fig. 8 for an InAs/GaAs quantum dot in the magnetic field, obtained by the 6×6 nonsymmetrized multiband Hamiltonian.

Inclusion of strain in the analysis leads to a splitting of the heavy- and light-hole bands,[30,31] which, consequently, decreases band mixing and partially suppresses the discussed effect because of the incorrect boundary conditions used in the conventional $\mathbf{k}\cdot\mathbf{p}$ theory.

V. SUMMARY AND CONCLUSIONS

A nonsymmetrized eight-band Hamiltonian for nanostructures is extended to include a magnetic field. The Hamiltonian is applied to the case of a parabolic confined cylindrical quantum dot in a perpendicular magnetic field. In general, we found that the agreement between our nonsymmetrized model and the conventional models strongly depends on the difference in the structural parameters between the quantum dot and the barrier material. For systems with a large difference in Luttinger parameters between the dot and barrier material, band mixing in the conventional model is found to be overestimated, and a good agreement between the single-band model and the nonsymmetrized multiband model was observed for the ground state. Comparing the energy levels as a function of magnetic field in the case of InAs/GaAs quantum dot to energy levels as a function of k_t for InAs/GaAs quantum well, a similar nonphysical behavior is demonstrated and is a direct consequence of the inappropriate treatment of the boundary. However, the question of an appropriate treatment of the interface in the general framework of envelope-function approximations is open for further studies.

ACKNOWLEDGMENTS

This work was supported by the Flemish Science Foundation (FWO-Vl), the Belgian Science Policy, the "Onderzoeksraad van de Universiteit Antwerpen" (GOA), the European Commission (EU) GROWTH programme NANOMAT

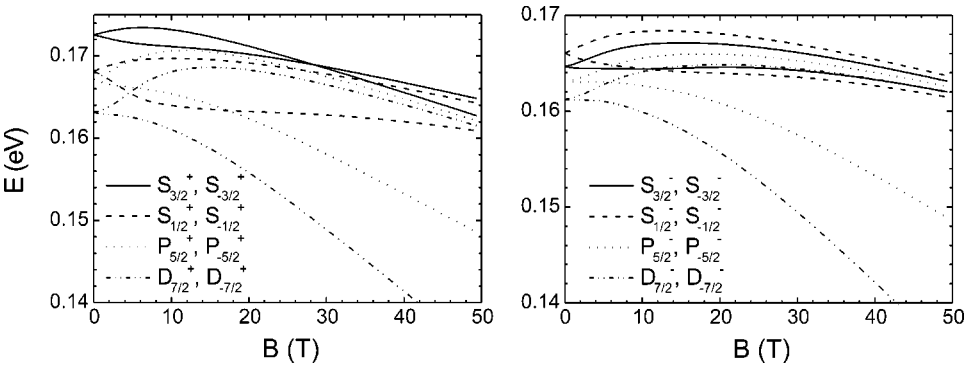

FIG. 8. The lowest-hole energy levels for 16 different symmetries as a function of the magnetic field in an InAs/GaAs quantum dot: $\hbar\omega_0 = 10$ meV and $h = 10$ nm. The results are given for the 6×6 nonsymmetrized multiband Hamiltonian.

project (Contract No. G5RD-CT-2001-00545), and the EU-NoE: SANDiE.

APPENDIX: STRAINED SEMICONDUCTING NANOSTRUCTURES

In the case of strained semiconducting heterostructures in a magnetic field an additional strain-dependent part should be added to the heterostructure Hamiltonian

$$H = H_k + H_s, \tag{A1}$$

where H_k denotes the kinetic part given by Eq. (9) and H_s is the strain-dependent part.

As adapted from Ref. 16, the strain Hamiltonian in the basis given in Eq. (8) becomes

$$\hat{H}_s = \begin{pmatrix}
a_c e & 0 & -i\sqrt{3}v^\dagger & -\sqrt{2}u & -iv & 0 & -iu & -\sqrt{2}v \\
0 & a_c e & 0 & v^\dagger & -i\sqrt{2}u & \sqrt{3}v & -i\sqrt{2}v^\dagger & u \\
i\sqrt{3}v & 0 & -p-q & is & r & 0 & -\frac{1}{\sqrt{2}}s & -i\sqrt{2}r \\
-\sqrt{2}u & v & -is^\dagger & -p+q & 0 & r & i\sqrt{2}q & -\sqrt{\frac{3}{2}}s \\
iv^\dagger & i\sqrt{2}u & r^\dagger & 0 & -p+q & -is & -\sqrt{\frac{3}{2}}s^\dagger & i\sqrt{2}q \\
0 & \sqrt{3}v^\dagger & 0 & r^\dagger & is^\dagger & -p-q & -i\sqrt{2}r^\dagger & -\frac{1}{\sqrt{2}}s^\dagger \\
iu & i\sqrt{2}v & -\frac{1}{\sqrt{2}}s^\dagger & -i\sqrt{2}q & -\sqrt{\frac{3}{2}}s & i\sqrt{2}r & -a_v e & 0 \\
-\sqrt{2}v^\dagger & u & i\sqrt{2}r^\dagger & -\sqrt{\frac{3}{2}}s^\dagger & -i\sqrt{2}q & -\frac{1}{\sqrt{2}}s & 0 & -a_v e
\end{pmatrix}, \tag{A2}$$

where

$$p = a_v(e_{xx} + e_{yy} + e_{zz}), \tag{A3a}$$

$$q = b\left[e_{zz} - \tfrac{1}{2}(e_{xx} + e_{yy})\right], \tag{A3b}$$

$$r = \tfrac{\sqrt{3}}{2}b(e_{xx} + e_{yy}) - ide_{xy}, \tag{A3c}$$

$$s = -d(e_{xz} - ie_{yz}), \tag{A3d}$$

$$u = \tfrac{1}{\sqrt{3}}P_0 \sum_j e_{zj}k_j, \tag{A3e}$$

$$v = \tfrac{1}{\sqrt{6}}P_0 \sum_j (e_{xj} - ie_{yj})k_j, \tag{A3f}$$

In the previous equations a_v is the hydrostatic valence-band deformation potential; a_c the conduction-band deformation potential; e_{ij} is the strain tensor, where i,j runs over x,y,z; and b and d are the shear deformation potentials.

*Electronic address: vladan.mlinar@ua.ac.be
†Permanent address: Faculty of Electrical Engineering, University of Belgrade, P.O. Box 3554, 11120 Belgrade, Serbia.
‡Electronic address: francois.peeters@ua.ac.be

[1] E. O. Kane, J. Phys. Chem. Solids **1**, 249 (1957).
[2] M. H. Weiler, R. L. Aggarwal, and B. Lax, Phys. Rev. B **17**, 3269 (1978); M. H. Weiler, in *Semiconductors and Semimetals*, edited by R. K. Willardson and A. C. Beer (Academic Press, New York, 1981), Vol. 16, Chap. 3, p. 119.
[3] J. M. Luttinger and W. Kohn, Phys. Rev. **97**, 869 (1955).
[4] J. M. Luttinger, Phys. Rev. **102**, 1030 (1956).
[5] C. R. Pidgeon and R. N. Brown, Phys. Rev. **146**, 575 (1966).
[6] R. Eppenga, M. F. H. Schuurmans, and S. Colak, Phys. Rev. B **36**, 1554 (1987).
[7] M. G. Burt, J. Phys.: Condens. Matter **4**, 6651 (1992).
[8] M. G. Burt, J. Phys.: Condens. Matter **11**, 53 (1999).
[9] B. A. Foreman, Phys. Rev. Lett. **80**, 3823 (1998).
[10] B. A. Foreman, Phys. Rev. B **48**, R4964 (1993).

[11] P. N. Stavrinou and R. van Dalen, Phys. Rev. B **55**, 15 456 (1997).
[12] E. P. Pokatilov, V. A. Fonoberov, V. M. Fomin, and J. T. Devreese, Phys. Rev. B **64**, 245328 (2001).
[13] A. V. Rodina, A. Yu. Alekseev, Al. L. Efros, M. Rosen, and B. K. Meyer, Phys. Rev. B **65**, 125302 (2002).
[14] E. L. Ivchenko, A. Yu. Kaminski, and U. Rössler, Phys. Rev. B **54**, 5852 (1996).
[15] B. A. Foreman, Phys. Rev. Lett. **81**, 425 (1998).
[16] F. Szmulowicz, H. Haugan, and G. J. Brown, Phys. Rev. B **69**, 155321 (2004).
[17] B. A. Foreman, cond-mat/0312713 (unpublished).
[18] A. T. Meney, B. Gonul, and E. P. O'Reilly, Phys. Rev. B **50**, 10 893 (1994).
[19] U. Bockelmann and G. Bastard, Phys. Rev. B **45**, 1688 (1992); **45**, 1700 (1992).
[20] O. Stier, M. Grundmann, and D. Bimberg, Phys. Rev. B **59**, 5688 (1999).
[21] C. Pryor, Phys. Rev. B **57**, 7190 (1998).
[22] C. Pryor, Phys. Rev. B **60**, 2869 (1999).
[23] M. Tadić, F. M. Peeters, and K. L. Janssens, Phys. Rev. B **65**, 165333 (2002).
[24] M. Hayne, J. Maes, Y. M. Manz, O. G. Schmidt, K. Eberl, and V. V. Moshchalkov, Appl. Phys. Lett. **79**, 45 (2001); M. Hayne, J. Maes, S. Bersier, V. V. Moshchalkov, A. Schilwa, L. Müller-Kirsch, C. Kapteyn, R. Heitz, and D. Bimberg, *ibid.* **82**, 4355 (2003).
[25] B. A. Foreman, Phys. Rev. B **56**, R12 748 (1997).
[26] It is assumed that inversion asymmetry of the zinc-blende lattice can be neglected.
[27] F. B. Pedersen and Y. C. Chang, Phys. Rev. B **53**, 1507 (1996).
[28] F. B. Pedersen and Y. C. Chang, Phys. Rev. B **55**, 4580 (1997).
[29] I. Vurgaftman, J. R. Meyer, and L. R. Ram-Mohan, J. Appl. Phys. **89**, 5815 (2001).
[30] S. L. Chuang, Phys. Rev. B **43**, 9649 (1991); Calvin Yi-Ping Chao and S. L. Chuang, *ibid.* **46**, 4110 (1992).
[31] B. A. Foreman, Phys. Rev. B **49**, 1757 (1994).